2023 18th Conference on Ph.D Research in Microelectronics and Electronics (PRIME) | 979-8-3503-0320-9/23/$31.00 ©2023 IEEE | DOI: 10.1109/PRIME58259.2023.10161773

Self-Adaptation of Line Driver Pre-Emphasis Parameters via Embedded Line Loss Sensing

Nicholas St. John[1], Soumyajit Mandal[1], Eric Raguzin[1], Piotr Maj[1], and Grzegorz W. Deptuch[1]
[1]Instrumentation Division, Brookhaven National Laboratory, Upton, New York 11973
Emails: {nstjohn, smandal, eraguzin, gdeptuch, pmaj}@bnl.gov

***Abstract*—The paper proposes a method for automated optimization of line driver pre-emphasis parameters by utilizing the measured transfer function (TF) of the channel. Pulse-echo measurements are performed in which pulses with a given frequency and duration are transmitted into the channel and the amplitude of the resulting echo detected to evaluate frequency-dependent line loss. The echo amplitude is indirectly detected using transmit pulses with different amplitudes and a simple comparator-based circuit that detects when the echo amplitude exceeds a user-defined threshold. The result is used to estimate the cable loss, and the process repeated for different input frequencies to estimate the channel TF. The proposed estimation procedure is validated using a transistor-level implementation in 65 nm CMOS for data rates up to 1 Gb/s, channel losses up to 15 dB, and a receiver reflection coefficient of -20 dB.**

***Index Terms*—component, formatting, style, styling, insert**

I. Introduction

All physical wired communication channels have transfer functions (TFs) with low-pass characteristics. Thus, as data rates continue to increase, the attenuation of signals through such channels (e.g., cables, PCB traces, and bond wires) is becoming more pronounced. The resulting frequency dispersion generates inter-symbol interference (ISI) in the received signal, increasing the bit-error rate (BER). ISI can be mitigated via pre-emphasis or feed-forward equalization (FFE), which manipulates the transmitted symbol shapes to sharpen transitions in the received signal. The effect of pre-emphasis in the frequency domain is to increase high-frequency content in the transmitted signal, canceling the low-pass cable TF [1].

Pre-emphasis is normally implemented via a finite impulse response (FIR) filter with N taps. The example shown in Fig. 1(a) uses $K = 3$ taps that are known as the pre-cursor, main-cursor and post-cursor, respectively. Only the weights of these taps are usually adjustable, while their relative delays are fixed to one clock cycle (i.e., $1\times$UI). In recent work, we have shown that the range of FFE transfer functions can be expanded by also allowing the relative time delays between the taps to be programmable [2]. The generic output waveform of such an adaptive driver is shown in Fig. 1(b). The parameters of the filter (in this case, three weights and two relative delays) determine the spectrum of the transmitted signal. ISI is minimized when the transmit spectrum approximates the inverse of the cable TF, thus ensuring that the received spectrum is flat within the bandwidth of interest (typically, at least $1/$UI) as shown in Fig. 2(a). Obtaining such a flat-band response

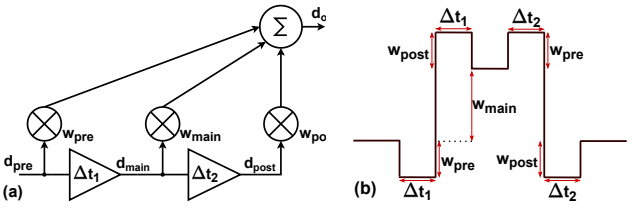

Fig. 1. (a) Example implementation of pre-emphasis via a three-tap FIR filter. (b) Generic bit shape generated by the FIR filter.

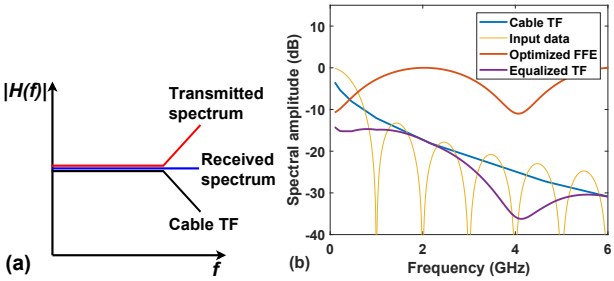

Fig. 2. (a) In an ideal case, pre-emphasis inverts the channel TF such that the spectrum of received data becomes flat within the transmit bandwidth. (b) A more realistic example, showing the use of a $K = 3$ tap FFE to invert the TF of a 2 m long radio-pure stripline fabricated on a flexible PCB.

requires the cable TF to be known; in this case the optimum FIR filter coefficients can be derived via an optimization procedure (see Fig. 2(b) for an example). Alternatively, it is also possible to find these optimum pre-emphasis parameters via an exhaustive search. However, neither method is feasible in practice since 1) the cable TF is not known, and 2) an exhaustive search is too time-consuming. Thus, this paper focuses on developing an automated method to obtain optimal FFE parameters for an arbitrary channel.

Earlier self-adaptive line drivers have attempted to solve this problem by automatically adjusting their source impedance to improve matching for different transmission lines [3]. In addition, auxiliary feedback information from the receiver (e.g., the measured BER) has been used for autonomous optimization of the driver's output voltage swing [4].

Here we propose a novel calibration method for line drivers with configurable pre-emphasis. Our approach uses on-chip line loss sensing to autonomously find the optimal transmit parameters for driving the cable, i.e., the waveform which minimizes power consumption while ensuring acceptable BER.

The rest of the paper is divided into four sections. Section II describes the optimization methodology, while Section III describes a transistor-level implementation of the proposed scheme. Section IV discusses simulated results obtained from the implementation, while Section V summarizes our contributions and discusses future work.

II. Optimization Scheme

The proposed scheme has two main steps, namely *transfer function measurement* and *figure of merit (FoM) minimization*, as seen in Fig. 3(a). Unlike earlier work [5], the cable TF is only measured from the driver side, thus eliminating the need for communication with the receiver. For this purpose, the cable is driven by a periodic waveform centered around a frequency ω_{in}. Assuming non-zero impedance mismatch between the cable and load, which is a safe assumption for practical systems, a fraction of the signal is reflected towards the driver from the receiver to form an echo. The amplitude of this signal is given by $v_{echo}(\omega_{in}) = |H(\omega_{in})|^2 \Gamma_L v_{TX}(\omega_{in})$ where $H(\omega_{in})$ is the transfer function of the cable, Γ_L is the reflection coefficient at the receiver, and $v_{TX}(\omega_{in})$ is the transmit signal amplitude. Since the output amplitude of the driver is known, we can estimate the frequency-dependent TF of the cable, $H(\omega)$, by measuring the received echo amplitude for different values of ω_{in}. Obviously, this estimate is only quantitative if Γ_L is known, for example if the receiver (which is matched during normal operation) is purposefully mismatched during calibration. However, even if Γ_L is unknown, our measurement will be approximately proportional to $H(\omega)$ as long as the frequency dependence of Γ_L is relatively weak, thus providing enough information to determine the optimal FFE coefficients (i.e., pre-emphasis parameters).

As for other pulsed measurements (such as time-domain reflectometry, radar, and ultrasound), the choice of transmit waveform is governed by a trade-off between frequency and time resolution. Specifically, narrowband waveforms provide high frequency resolution but have poor temporal resolution, while broadband waveforms are the reverse. Moreover, the received signal-to-noise ratio (SNR) is proportional to signal energy, and thus increases with waveform length. Since our primary goal is to reconstruct the cable TF, $H(\omega)$, narrowband waveforms such as continuous wave (CW) tones are preferable. However, detecting weak echo signals in the presence of such a CW transmission requires complex duplexer circuits [6]. To avoid the need for duplexers, we implement a pulsed measurement scheme using N-cycle tone bursts (i.e., a repeating $0101\ldots..$ bit pattern with a bit period of $T = \pi/\omega_{in}$). The bandwidth of such a pulse is $\approx \omega_{in}/N$, thus allowing the value of N to be adjusted to provide an appropriate trade-off between resolution and SNR. Note that the cable should be long enough for its propagation delay to exceed the duration of the pulse train. A Fourier analysis shows that the amplitude of the fundamental component (at ω_{in}) is $4/\pi \approx 2.1$ dB larger than that of the peak. Also note that the resulting spectrum is a sinc function, which has relatively high sidelobes. If required, the amplitude profile can be modified to a smoother function, such as triangular or Hamming-like, to reduce the sidelobe level.

The proposed scheme relies on performing swept-amplitude pulse-echo measurements. In other words, the driver generates pulses with monotonically increasing amplitudes and monitors the amplitudes of the resulting echoes. Rather than measuring the exact amplitude of each echo in the sweep, which would require a prohibitively power-hungry ADC, we instead use a low-power comparator to sense the echoes. The comparator uses built-in hysteresis to ensure that it is only triggered when the echo amplitude exceeds an input-referred threshold voltage, V_{MIN}. The sweep is stopped and the current transmit amplitude, V_{TX}, recorded once the comparator detects the echo, thus enabling $|H(\omega_{in})|^2\Gamma_L$ to be indirectly estimated as the ratio $V_{MIN}/v_{TX}(\omega_{in})$. Specifically, since v_{TX} is determined via the driver amplitude setting, which is known, the desired transfer function is inversely proportional to the square root of the value of v_{TX} at which the echo is first detected. Assuming M-bit amplitude control, the dynamic range (DR) for channel TF sensing is $2^{M/2} \approx 3M$ dB. Thus 5-bit control provides a DR of ≈ 15 dB, which is sufficient to determine pre-emphasis parameters for the channels of interest.

Fig. 3(b) shows a simplified block diagram of the proposed adaptive line driver. The design, which is implemented in standard 65 nm CMOS technology, is intended for data transfer in cryogenic environments (77K and above) at rates up to 1 Gb/s [2]. It uses a current-mode (CML) driver with programmable bias current (controlled by the digital word $SWING$) to generate the probe pulses. While voltage-mode drivers can consume up to $4\times$ less power then CML for the same swing, they are difficult to use with pre-emphasis since their output swing and output impedance are strongly coupled. By adjusting their swing based on measured line loss, adaptive CML drivers can thus consume less power than voltage-mode equivalents for low- and moderate-loss cables.

The reflected echo is amplified and thresholded by a hysteretic comparator. A digital counter enabled after the output pulse is sent is used to estimate N_{comp}, the number of edges present in the comparator output. This number is compared with a user-set minimum count value, N_{MIN}. The echo is assumed to have been detected (resulting in OUT going high) only if $N_{comp} \geq N_{MIN}$. The value of N_{MIN} can be adjusted to trade-off between robustness to noise (higher N_{MIN}) and sensitivity (lower N_{MIN}).

III. Circuit Implementation

The performance of the proposed cable TF measurement system is largely limited by that of the comparator, which should have a high gain-bandwidth product to ensure adequate sensitivity over the desired range of data rates. Also, its input-referred threshold, V_{MIN}, should be set to a level that is 1) high enough to avoid being triggered by noise, and 2) low enough to ensure that weak echoes can be detected. Sensitivity is thus maximized for a noise-dependent value of V_{MIN}; this is an example of stochastic resonance (SR) [7], a well-known phenomenon in which the response of a nonlinear

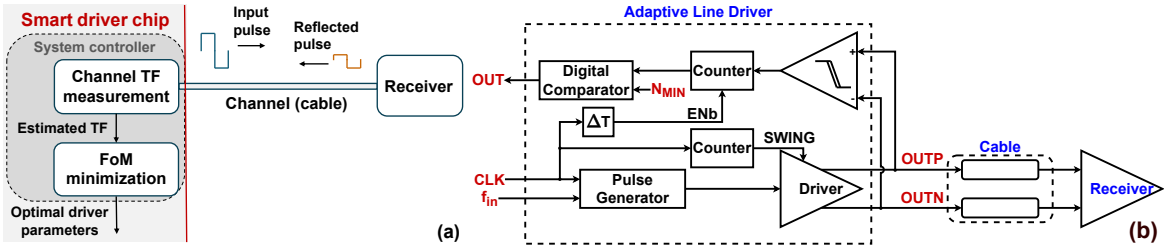

Fig. 3. (a) Block diagram of the proposed self-optimized "smart" line driver. (b) Block diagram of the circuit used for cable TF measurement.

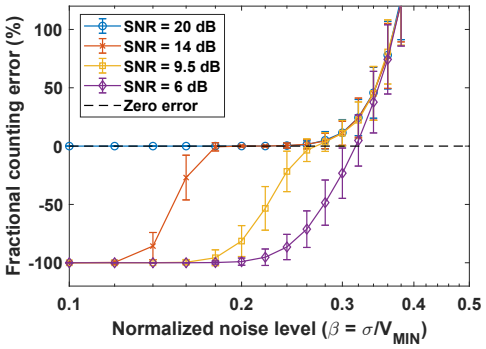

Fig. 4. Fractional counting error of the hysteretic comparator as a function of normalized noise level, β, for several values of input SNR. Error bars denote ± 1 standard deviation after 500 trials.

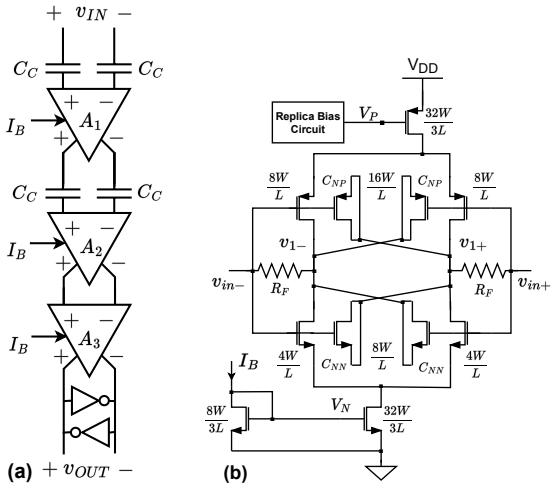

Fig. 5. (a) High-level schematic of the proposed hysteretic comparator. (b) Schematic of the first stage (A_1). Stages #2 and #3 are identical apart for the addition of a cross-coupled inverter pair (i.e., latch) in stage #3.

system to a weak periodic input signal is optimized by the presence of a particular, non-zero level of noise. For low noise levels, weak signals cannot cross the threshold of the bistable element (hysteretic comparator), so little signal passes through it and output SNR is low. For high noise levels, the output is dominated by the noise, also leading to low output SNR. At moderate levels, the noise is large enough to allow the signal to cross the threshold but not large enough to dominate the output, thus maximizing output SNR. As described in [8], the dynamics are defined by two dimensionless parameters: the normalized input signal amplitude $\alpha = v_{echo}/V_{MIN}$ and the normalized (rms) noise level $\beta = \sigma/V_{MIN}$. Note that the input SNR (in rms units) is given by $v_{echo}/\sigma = \alpha/\beta$.

Let us denote the number of signal edges detected by the comparator by N_{comp}, and recall that the desired (or ideal) number is $2N$. Fig. 4 shows the fractional counting error $\epsilon_{comp} \equiv (N_{comp}/2N - 1)$ versus β for several values of input SNR. For high SNR (20 dB in this plot), noise is not required to detect the signal, so $\epsilon_{comp} = 0$ for values of $\beta < 0.25$ before gradually increasing due to generation of spurious edges. For intermediate SNR values (14 and 9.5 dB in this plot), we observe noise-assisted signal detection, as predicted by SR. Specifically, note that $\beta \approx 0.25$ is optimal in the sense that it enables $\epsilon_{comp} \approx 0$ to be obtained at the lowest possible input SNR (9.5 dB in this case). Finally, for low SNR (6 dB in this plot), the added noise is too large to be useful and low counting error (i.e., $\epsilon_{comp} \approx 0$) cannot be obtained.

Fig. 5(a) shows a high-level schematic of the proposed comparator. The design consists of three fully-differential amplifiers (A_1, A_2, and A_3). The use of multiple gain stages ensures a high gain-bandwidth product. The first two stages are AC-coupled to reject unwanted low-frequency signals, such as common-mode shifts. The third stage includes a weak latch (cross-coupled inverter pair) to generate a moderate amount of hysteresis, V_H. The value of V_H can be adjusted via the strength of the latch. Fig. 5(b) shows the schematic of the first stage. The circuit uses complementary (inverter-like) input pairs to allow current reuse, which in turn results in higher transconductance and lower input-referred noise. The PMOS bias voltage, V_P, is set by a replica circuit (not shown), while the MOS capacitors C_{NP} and C_{NN} are used to neutralize the nonlinear differential-mode capacitance of the input pairs.

For a bias current of $I_B = 800$ μA, the combined small-signal gain of the two pre-amplification stages is 34.4 dB with a -3 dB bandwidth of 0.12-1.30 GHz. Thus, the overall gain varies by only 0.8 dB over the desired operating bandwidth of 0.15-1.0 GHz, making it unnecessary to compensate for frequency-dependent comparator gain. The input-referred in-band noise PSD and total output noise are $\overline{v_{n,in}^2} \approx 2.3$ nV/Hz$^{1/2}$ and $\sigma_{out} = 20.6$ mV$_{rms}$, respectively. Thus, the total input-referred noise for in-band frequencies is

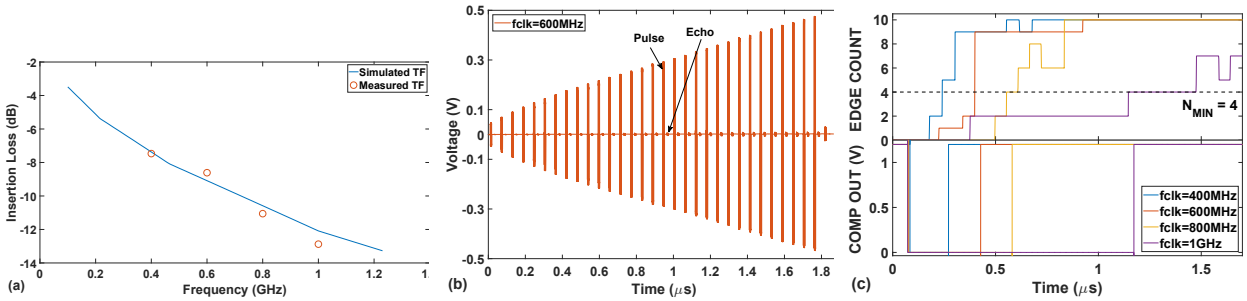

Fig. 6. (a) Estimated and actual insertion loss for a 2 m flexible low-mass stripline cable. (b) Line driver output amplitude sweep at a center frequency of 600 MHz. (c) Edge counter and edge count threshold comparator outputs for the 2 m long cable at different center frequencies.

$\approx 90\ \mu V_{rms}$. The hysteresis level is set to $V_H \approx 140$ mV, resulting in an input-referred threshold of $V_{MIN} \approx 0.37$ mV. The corresponding value of $\beta \approx 0.24$ is almost independent of frequency and close to the optimum shown in Fig. 4.

IV. Results

Since the duty cycle of the driver is low, the power consumption of the TF measurement system is dominated by the comparator. For the nominal $I_B = 800\ \mu$A, the entire system consumes ~2.5 mA from a 1.5 V supply. Note that the system can be powered down once the measurement is complete, i.e., does not increase power consumption during normal operation.

The accuracy of the proposed method was tested by designing and simulating the entire channel TF measurement block at the transistor level using TSMC 65 nm device models. Pulse widths were set to $N = 5$ cycles, resulting in an ideal comparator output count value of $N_{comp} = 10$. The output amplitude of the CML driver was linearly increased with $M = 5$ bit resolution using a current DAC, resulting in an output amplitude step size of $\Delta V_{TX} \approx 14.4$ mV and a peak amplitude of ≈ 0.46 V into a matched load. Four simulations run at different frequencies ranging from (0.4 - 1) GHz. In each case, the output value, $SWING$, of the counter that controls the CML driver amplitude was recorded when the detected edge count of the comparator reaches $N_{MIN} = 4$.

In order to estimate the channel loss, we find the reciprocal of the $SWING$ value, take its square root, and then convert the result to dB. In practice, these computations can be replaced by a small lookup table (LUT). In either case, since Γ_L is generally unknown, the results are scaled to match the actual or simulated TF of the cable via a one-point calibration method. The results of this process are shown in Fig. 6(a) for a 2 m long flexible low-mass stripline cable (designed for use within a time projection chamber) and $\Gamma_L = -20$ dB. The figure shows that 1) the measured TF from the testbench is a good approximation to the actual channel TF, and 2) only a few data points across the operating frequency range are required to obtain an accurate estimate of the slope of the channel TF, $d(|TF(\omega)|/d\omega$, which is the main input required to optimize the FFE coefficients. Also note that the one-point calibration step is only required for display purposes, and does not need to be performed in order to estimate $d(|TF(\omega)|/d\omega$.

The driver output showing the amplitude sweep and the digital outputs (edge counter and edge count threshold) of the block are shown in Figs. 6(b) and 6(c), respectively. Note that the edge counter starts to increase progressively later during the sweep as the input frequency increases, as expected due to the increase in cable insertion loss.

V. Conclusion

This paper has presented an embedded self-calibration method for minimizing the power consumption (or more generally, a suitable FoM) of line drivers with programmable pre-emphasis. Compared to the state of the art, this is the first to include TF estimation at the transmitter. The proposed technique is particularly suitable for obtaining "plug-and-play" functionality, i.e., enabling the driver to automatically estimate the optimal single-bit waveform for driving any channel. The technique, implemented in 65 nm CMOS, can be readily extended to drivers with higher data rates and/or multi-bit outputs (e.g., using PAM-4 encoding). Future work will focus on 1) experimental validation using a variety of channels; and 2) digitizing the pulse propagation delay, allowing the phase and group delay of the cable TF to also be measured.

References

[1] J. Jiang, W. He, J. Wei, Q. Wang, and Z. Mao, "Design optimization for capacitive-resistively driven on-chip global interconnect," *IEICE Electronics Express*, vol. 12, no. 8, pp. 20 150 111–20 150 111, 2015.

[2] N. S. John, S. Mandal, G. W. Deptuch, E. Raguzin, and S. Rescia, "A low-power 1 Gb/s line driver with configurable pre-emphasis for lossy transmission lines," *Journal of Instrumentation*, 2023.

[3] B. Nauta and M. B. Dijkstra, "Analog line driver with adaptive impedance matching," *IEEE Journal of Solid-State Circuits*, vol. 33, no. 12, pp. 1992–1998, 1998.

[4] S. M. PD, H. Yu, H. Huang, and D. Xu, "A Q-learning based self-adaptive I/O communication for 2.5D integrated many-core microprocessor and memory," *IEEE Trans. Computers*, vol. 65, no. 4, pp. 1185–1196, 2015.

[5] D. Xu, S. M. PD, H. Huang, N. Yu, and H. Yu, "An energy-efficient 2.5D through-silicon interposer I/O with self-adaptive adjustment of output-voltage swing," in *Proc. 2014 ISLPED*, 2014, pp. 93–98.

[6] C. Yuan, A. Naguib, and S. Shekhar, "On the design of low-power hybrids for full duplex simultaneous bidirectional signaling links," *IEEE Trans. Circ. and Systems I: Regular Papers*, vol. 67, no. 4, pp. 1413–1422, 2020.

[7] L. Gammaitoni, P. Hänggi, P. Jung, and F. Marchesoni, "Stochastic resonance," *Rev. Mod. Phys.*, vol. 70, no. 1, pp. 223–287, Jan. 1998.

[8] P. Dehghanzadeh, H. Zamani, S. Shaik, and S. Mandal, "A wireless implantable microsystem for real-time bladder volume monitoring," *TechRxiv*, 2022.